# High-Resolution, Nonmechanical Approach to Polarization-Dependent Transmission Measurements

Rex M. Craig, Sarah L. Gilbert, *Member, OSA,* and Paul D. Hale, *Member, OSA*

*Abstract*—**We have implemented an automated, nonmechanical approach to the measurement of polarization dependent loss (and, equivalently, gain). We use a deterministic fixed-states method to derive Mueller matrix elements from intensity measurements at specific polarization states. Voltage-modulated liquid-crystal variable retarders set the polarization states. Synchronous detection is employed to increase the signal-to-noise ratio (SNR) of the system and thereby allow measurement resolution to better than 0.001 dB. We present polarization-dependent loss measurements from 0.0016 to 0.56 dB at 1550 nm to verify performance.**

*Index Terms*—**Liquid-crystal retarders, liquid-crystal variable retarders, Mueller matrix, polarization dependence, polarization-dependent loss (PDL), polarization-dependent transmission, synchronous detection.**

## I. Introduction

POLARIZATION-dependent loss (PDL) and gain, which together we call polarization dependent transmission, are important considerations in both digital [1], [2] and analog [3] networks due to increases in the bit error rate (BER) and signal distortion, respectively. The push toward all-optical networks has increased pressure to reduce component PDL. PDL is primarily a characteristic of single-mode systems for which the signal is highly polarized but of variable state. It is defined as $10\log(T_{\max}/T_{\min})$ (in dB) where $T$ is transmittance taken over the entire polarization-state space. This space is most readily visualized with the aid of the polarization (Poincaré) sphere [4], [5]. Often degradation caused by PDL is modified by polarization mode dispersion in complex ways [6]. Polarization dependent loss and gain are usually characterized as localized component effects as opposed to the distributed nature of polarization mode dispersion.

Our goal is to establish the capability to measure PDL with a resolution of better than 0.001 dB and to determine the absolute accuracy of our method. This may lead to an artifact standard for the calibration of commercial instrumentation. This paper describes a new approach to polarization dependent transmission measurement that employs a nonmechanical technique capable of synchronous detection.

We divide PDL measurement techniques into three rough categories, all of which are represented by commercial instrumentation: deterministic all-states, pseudorandom all-states, and deterministic fixed-states. The term "deterministic all-states" refers to techniques that span a large subset of the entire polarization-state space (as represented by the Poincaré sphere) in a repeatable way. This method spans the Poincaré sphere along predetermined trajectories to produce a good approximation of full sphere coverage. This may be done by rotating a retarder pair in a well-defined phase relationship [7], [8]. Laboratory devices based on this concept have reported repeatability of ±0.003 dB and resolution of 0.001 dB [9] while commercial devices have a specified repeatability of ±0.010 dB and resolution of 0.001 dB. An advantage of this approach is high speed since the optics can be rotated at high velocity as long as the proper phase relationship is maintained. Accuracy, however, requires a very high degree of mechanical precision, correction of strong wavelength dependence, and low internal PDL. Resolution is a function of the degree of sphere coverage and the signal-to-noise ratio (SNR).

The term "pseudorandom all-states" refers to techniques that span a large subset of the entire Poincaré sphere through a pseudorandom variation of retardance, usually the distributed retardance of optical fiber loops [8], [10]. This method has the advantage of low system noise, weak wavelength dependence, and low internal PDL since the beam remains confined in a single-mode fiber. On the other hand, this is a statistical sampling technique with accuracy dependent on the sampling rate and sampling time. Resolution is fundamentally limited by both the signal-to-noise ratio (SNR) and degree of Poincaré sphere coverage. Laboratory devices based on this idea have reported repeatability of ±0.001 [11] while commercial devices have specified repeatability of ±0.002 dB and resolution of 0.001 dB.

The term "deterministic fixed-states" refers to techniques that employ only three or four well-defined input states of polarization to derive global polarization dependence through some form of matrix analysis. Again, this technique typically employs bulk components in an open beam [8], [12], [13]. This method has the potential advantage of high speed and calibrated spectral dependence. Nonetheless, its accuracy is subject to mechanical precision as well as internal PDL. Resolution is not a function of sphere coverage but is fundamentally limited by the SNR. Laboratory devices based on this technique have reported repeatability in the range of ±0.001 to ±0.03 dB [12], [14] while commercial devices have specified repeatability of ±0.010 dB and resolution of 0.001 dB.

Because PDL is always greater than or equal to zero, noise in the PDL measurement system can degrade its sensitivity to very small PDL values (where the PDL is less than the

Manuscript received October 1, 1997; revised April 2, 1998.

The authors are with the National Institute of Standards Technology (NIST), Boulder, CO 80303 USA.

Publisher Item Identifier S 0733-8724(98)04828-2.

system's single-measurement noise). Sensitivity to these small PDL values cannot be improved by increasing the number of measurements; the average of multiple PDL measurements will always yield a positive value that is proportional to the single-measurement noise. However, averaging measured intensities in a deterministic fixed-states method can improve sensitivity.

We have chosen to implement a deterministic fixed-states technique using voltage-modulated liquid-crystal retarders and synchronous detection. Modulation of the polarization state allows differential measurement as well as an improvement in sensitivity due to averaging.

Four primary concepts will be presented in Section II. They are the basic matrix-method idea, the need for improvement through signal averaging, the advantages of a liquid crystal implementation, and potential disadvantages. Experimental implementation is discussed in Section III, and Section IV outlines an uncertainty analysis for our system. We present measurement results in Section V and draw conclusions in Section VI. Mathematical details are given in the Appendices.

## II. Concept

Our method, which we call the Mueller–Stokes technique, is a variation on a matrix technique developed by Favin *et al.* [13], which relies solely on power measurements. In this deterministic fixed-states method, four well-defined polarization states are necessary to determine the first-row Mueller matrix elements of a component. The global polarization dependence of transmittance can then be determined from these elements, as shown in Appendix A. This technique is under active consideration by both national and international standards committees as an acceptable alternative to the traditional deterministic all-states methods.

Because the measurement depends only on the relative coordinates of the four states, the only requirements on the set are that they maintain relative angular separations of 90° about the origin of the Poincaré sphere. This implies that intervening retardance, as represented by rotations of the sphere, will have no net effect. A representative sample of states in the laboratory frame would be, for example, vertical linear polarization, horizontal linear polarization, 45° (bisector) linear polarization, and right circular polarization as shown in Fig. 1(a), while a rotation of those states is shown in Fig. 1(b).

In our system, the polarization states are produced by two liquid crystal voltage regulator (LCVR) units [15] in series. These modulate the polarization state of a low-coherence polarized beam as in Fig. 2. The effect of the pair is to produce final polarization states equivalent to those produced by a quarter-wave and half-wave retarder combination undergoing independent rotations. Following generation of the four polarization states (with powers given by $I_a \cdots I_d$), the light is transmitted via single mode fiber with arbitrary but relatively stable birefringence through the device under test (DUT). It proceeds to a polarization-insensitive detector on which we measure the four output powers ($I_1 \cdots I_4$). We measure the input powers ($I_a \cdots I_d$) in the same way with the DUT removed to establish a baseline system response. The relationship of the output to input powers through the first row Mueller matrix elements ($m_{11} \cdots m_{14}$) of the DUT is given by

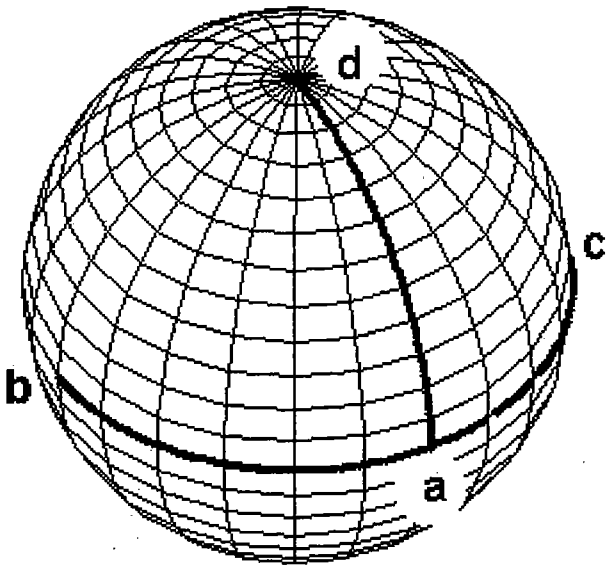


(a)

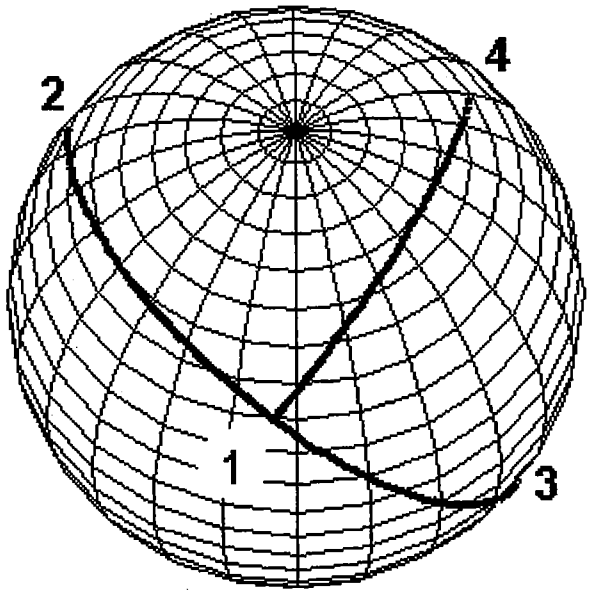


(b)

Fig. 1. (a) Poincaré trajectories for a given initial state of the LCVR Mueller–Stokes PDL measurement system and (b) Poincaré trajectories for the LCVR Mueller–Stokes PDL measurement system in the presence of fiber birefringence giving a $\pi/4$ retardance with fast axis at 11.25°.

$$\begin{bmatrix} I_1 \\ I_2 \\ I_3 \\ I_4 \end{bmatrix} = \begin{bmatrix} I_a & I_a & 0 & 0 \\ I_b & -I_b & 0 & 0 \\ I_c & 0 & I_c & 0 \\ I_d & 0 & 0 & I_d \end{bmatrix} \begin{bmatrix} m_{11} \\ m_{12} \\ m_{13} \\ m_{14} \end{bmatrix}. \tag{1}$$

The four first-row Mueller matrix elements are derived from an inversion that yields combinations of ratios of corresponding

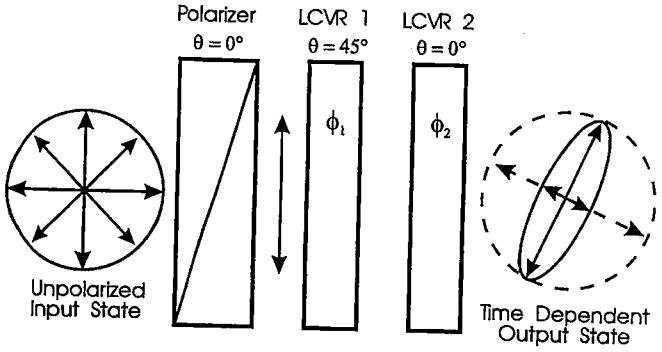


Fig. 2. Schematic representation of the LCVR Mueller–Stokes controller and polarization state evolution. Polarizer and retarder fast axes are given by $\theta$ (degrees) while retardance is represented by $\phi_1$ and $\phi_2$ (radians). The axes are fixed while retardance is time dependent.

powers

$$\begin{bmatrix} m_{11} \\ m_{12} \\ m_{13} \\ m_{14} \end{bmatrix} = \begin{bmatrix} \frac{1}{2}\left[\frac{I_1}{I_a} + \frac{I_2}{I_b}\right] \\ \frac{1}{2}\left[\frac{I_1}{I_a} - \frac{I_2}{I_b}\right] \\ -\frac{1}{2}\left[\frac{I_1}{I_a} + \frac{I_2}{I_b}\right] + \frac{I_3}{I_c} \\ -\frac{1}{2}\left[\frac{I_1}{I_a} + \frac{I_2}{I_b}\right] + \frac{I_4}{I_d} \end{bmatrix}. \tag{2}$$

Information about the global transmission extrema are contained in the first row matrix elements. Appendix A shows that the transmission extrema, $T_{\min}$ and $T_{\max}$, are

$$\begin{aligned} T_{\max} &= m_{11} + \sqrt{m_{12} + m_{13} + m_{14}} \\ T_{\min} &= m_{11} - \sqrt{m_{12} + m_{13} + m_{14}}. \end{aligned} \tag{3}$$

Polarization-dependent loss (in dB) is then defined as the ratio

$$\text{PDL} \equiv 10 \log \left[\frac{T_{\max}}{T_{\min}}\right]. \tag{4}$$

The input Stokes vector with unit power

$$S_{\text{in}}(\phi_1, \phi_2) = \begin{bmatrix} 1 \\ \cos(\phi_1) \\ \sin(\phi_1)\sin(\phi_2) \\ -\sin(\phi_1)\cos(\phi_2) \end{bmatrix} \tag{5}$$

is a function of LCVR retardance coordinates. The individual LCVR retardance coordinates ($\phi_1$ and $\phi_2$) represent unit 1 and unit 2. When we plot on the Poincaré sphere a subvector consisting of the last three elements against the phases as $\phi_1 = \pi/2 \cdots \pi$ (continuously) and $\phi_2 = \pi/2,\ \pi,\ 3\pi/2$ (discretely) we obtain the $T$ trajectory of Fig. 1(a). The endpoints and vertex of this trajectory define the ideal states of the Mueller–Stokes measurement: three along the equator (linear polarization) and one at the pole (circular polarization). In fact, due to intervening birefringence, one rarely observes such an aligned trajectory. The effect of birefringence is merely to rotate and translate the trajectory to another part of the sphere as demonstrated in Fig. 1(b) showing a constant $\pi/4$ retardance with fast axis at 11.25°. As long as the additional retardance is constant during the measurement, the results are independent of this retardance since calibration relies solely on arc lengths (assuming negligible detector PDL). This is demonstrated algebraically by noting the absence of loss terms in the first row of the ideal retardance matrix [Appendix B, (B2)].

The essential advantage of this technique is nonmechanical retardance modulation that allows rapid synchronous time averaging in a low noise environment. Synchronous time averaging improves the SNR and can be applied in different ways depending on the method of signal acquisition chosen. We have ruled out lock-in amplifier measurement as impractical since the signal is not a simple periodic function. The alternative is to average in the time domain with gated integration. We use a boxcar averager, though it could also be done with appropriate digital sampling.

Of the potential disadvantages, perhaps the most serious is the temperature dependence of the LCVR cells. The other is internal PDL of the retarder; we find this 0.02 dB offset to be unavoidable on one of the state transitions. Though this value is cancelled in the ratio calculations, drift could cause measurement error. Both effects can be minimized by passive or active temperature stabilization if necessary. Stability in system birefringence is important both during and between each set of power measurements and is assumed in the ideal case. Deviations from the ideal can be modeled as discussed later. An advantage of our technique is that the measurements can be done quickly, so the stability criterion is easy to satisfy.

Finally, there are two issues of concern in any PDL measurement: polarization dependence in the detector and depolarization within the DUT. Detector PDL can cause system PDL variation due to drift in the incident polarization state and distortion that arises from PDL superposition [16]. If the detected signal is highly depolarized before detection, then the stability requirement between baseline and DUT measurement sets is relaxed as the detector's own PDL is effectively eliminated. Erbium-doped fiber has been used to good effect as a depolarizer in this regard, though at a high cost in terms of signal power [11], [14]. We used a multimode fiber depolarizer [17]. The magnitude of these effects will be discussed further in Section IV. The issue of depolarization within the DUT is of concern in situations where the DUT exhibits polarization mode dispersion (PMD) prior to elements generating PDL. An example of this is a device that incorporates birefringent material. If the dispersion is sufficient to partially depolarize a short coherence source, relation (A2) is no longer valid and the PDL measurement result will depend on the source coherence. Although the study of PMD interaction with PDL is not within the scope of this paper, it is an important issue to keep in mind when measuring a device that has large PMD.

## III. Implementation

Fig. 3 shows a schematic of the measurement system. Our system consists of four major sections: source, LCVR cavity, detector, and control computer. The source is a 1550 nm edge-emitting light-emitting diode (ELED) operated in constant current mode. The pigtailed ELED emits approximately 20 $\mu$W out of a single-mode fiber. The short coherence length of this source ($\sim$40 $\mu$m) substantially reduces interference in the

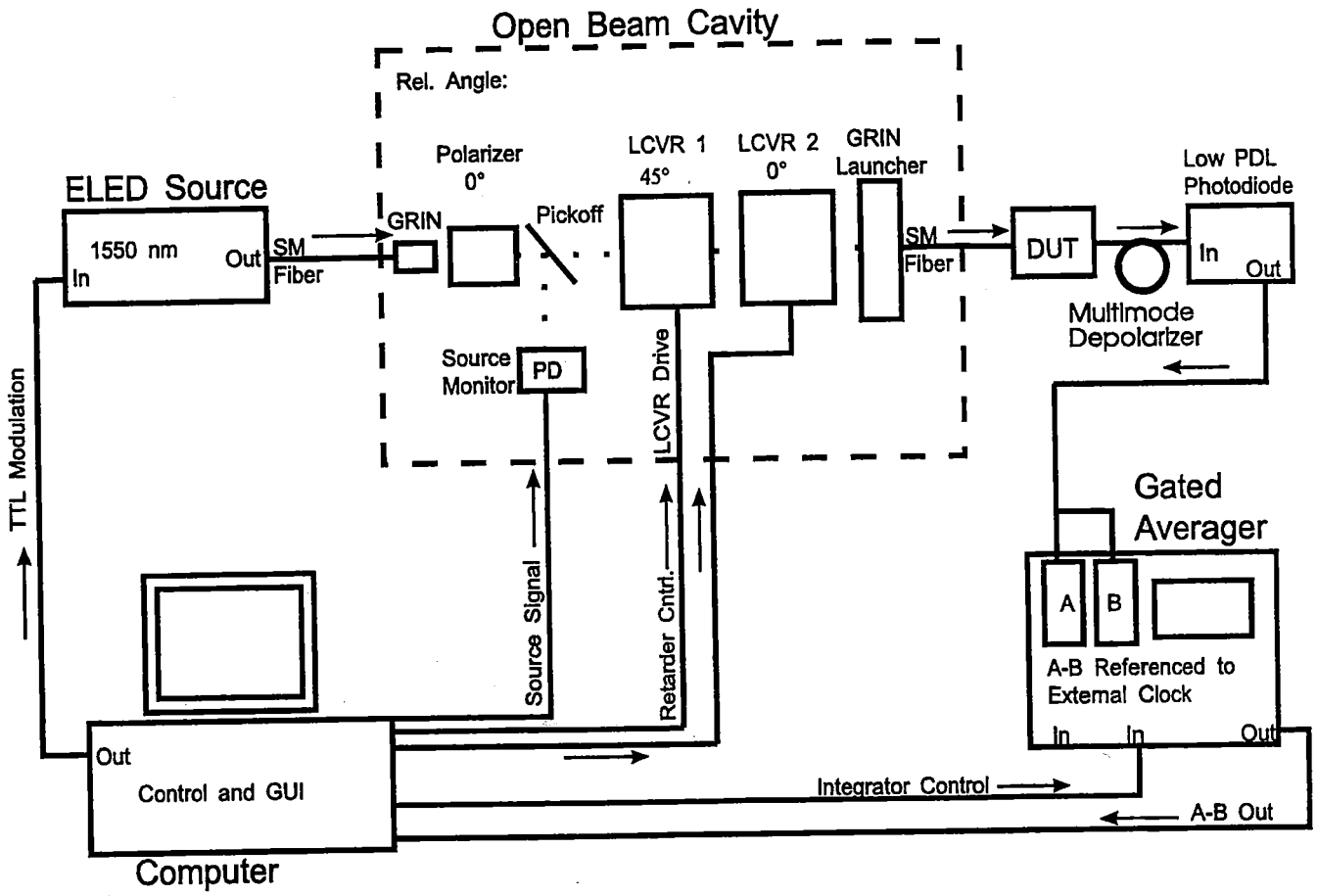


Fig. 3. Schematic of the LCVR PDL measurement system implementation.

optical path. The ELED light is collimated by a GRIN lens and then passed through a Glan–Thompson polarizer that acts to fix the polarization coordinate system. We tap this polarized light by a 5% beamsplitter and monitor it with an InGaAs photodetector that acts as the source monitor. The first LCVR unit is next, with fast axis at 45° to the incident polarization; the second LCVR follows with fast axis at 0°. The retardance as a function of the applied voltage for both devices is shown in Fig. 4. Each liquid crystal element was designed to provide up to $2\pi$ retardance modulation at a wavelength of 1600 nm. Relative retardance modulation spans either $\pi$ or $\pi/2$ depending on the unit; we operate the LCVR elements in the 1–4 V range. The final element is the pigtailed GRIN lens that launches light into the single-mode fiber. We connect this polarization-modulated light directly to the DUT without any intervening components other than fiber connectors. We find that connectors can introduce an additional PDL as discussed in Section IV; the cause and magnitude of this PDL are the subject of future investigation.

Measurements at each polarization state are limited to a fixed number $N$ of modulation cycles at clock frequencies of 3.5–10 Hz. To the extent that we can control birefringence drift during the sampling of each polarization state, resolution increases as $\sqrt{N}$. In addition, we use differential measurements to eliminate common-mode drift. Each of the three congruent line segments in Fig. 1 originating from the vertex

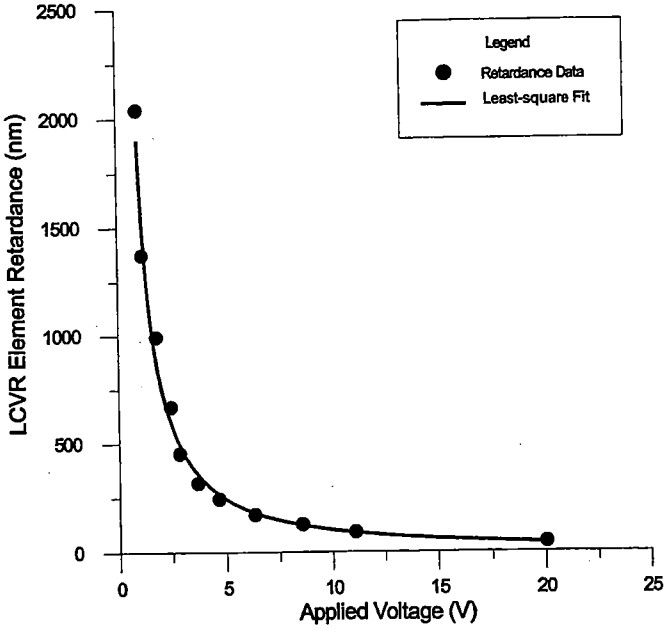


Fig. 4. Retardance response data for each of the LCVR elements used in this system along with a least-square fit to $1820/V^{1.25}$.

represents the modulation path between two Mueller–Stokes states and, therefore, a signal to be sampled. This signal is routed to two averager channels, and each channel has a delay

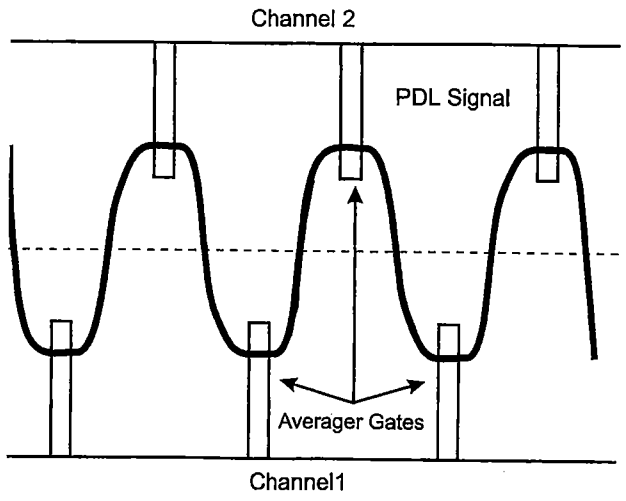


Fig. 5. Representation of the relationship between signal averager gating functions and an LCVR modulation signal (not drawn to scale).

set to position the respective gates on alternate periods as in Fig. 5. To obtain the proper Stokes powers, each of the three difference measurements must be subtracted from the absolute power of the central polarization state. Recall from Fig. 1 that this central state is equidistant from those other orthogonal states, in terms of arc length on the sphere. We measure the central state power by chopping the source at the clock frequency. Thus, the signal is fundamentally similar to the difference measurements and can be obtained with the same averager, thereby eliminating the need for an ac/dc calibration factor.

We use these three sets of averaged differences together with the chopped power measurement taken at the vertex state to recreate the four separate polarization state powers required by the Mueller–Stokes technique

$$I_0,\ I_1 = I_0 - \Delta I_{01},\ I_2 = I_0 - \Delta I_{02},\ I_3 = I_0 - \Delta I_{03} \quad (6)$$

where $I_0$ is the source power and $\Delta I_{01}$ through $\Delta I_{03}$ represent the three distinct polarization modulation signals. In this way, we maximize SNR improvement while minimizing the dynamic range. LCVR modulation along each segment trajectory takes place in short sequential bursts, each of which is internally averaged. We sample each internal average with 16 bits of resolution and average it with other samples over several repetitions. Thus, the effect of a slow drift in system birefringence is minimized without losing the improved signal-to-noise ratio advantage of synchronous detection.

Our measurement detector is a low-noise InGaAs element that is preceded by a multimode fiber depolarizer to effectively eliminate detector PDL. The depolarizer is a 45-m-long spool of 50/125 $\mu$m multimode fiber with a 0.37 numerical aperture. In separate tests, we find that it is capable of reducing the extinction ratio of linearly polarized incident light from about 40 to 0.4 dB.

Changes in the absolute power are divided out in real time using the source monitor signal. Detected signals are amplified and ac-coupled into both channels of the signal averager. We adjust the amplification gain remotely using a precise external signal attenuator to allow for both high and low modulation levels without overload. A central transistor–transistor logic (TTL) clock synchronizes both the computer and the gated integrator. Custom circuitry handles various chores associated with synchronizing the control, modulation, and sampling circuits at any frequency within the usable range. User input is entered through a graphical-user-interface that provides detailed control over all aspects of operation.

## IV. Uncertainty Analysis

The deviations from the ideal case have already been partially described above. They fall into three broad categories: temperature dependence, polarization state accuracy, and internal (system) PDL. Our estimates of these uncertainties along with total uncertainty computed for various cases (Type A and Type B [18]) are given in Table I. The uncertainties listed correspond to one standard uncertainty ($1\sigma$). Each uncertainty source in the table is discussed below.

### *A. Polarization State Uncertainty*

Polarization state accuracy depends on the accuracy of the calibrating polarimeter. In this case, we rely on the manufacturer's specifications of a $\pm 1.5°$ uncertainty in the coordinates of the polarization state. The uncertainty is manifested either in arc length along the sphere or deviation from orthogonality between the arcs during LCVR calibration. This uncertainty in the state implies a corresponding uncertainty in the matrix elements associated with any state.

### *B. Retarder Temperature Dependence*

We quantify temperature dependence primarily in terms of its effect on the LCVR elements. Again, we rely on the manufacturer's estimate of 0.4%/°C for the temperature coefficient of LCVR retardance. A worst-case temperature variation of 0.5 °C is used to derive the resulting uncertainty in signal power due to variation in the polarization state. For a rectangular distribution with upper and lower limits of ±0.2% about the mean value, this corresponds to a standard uncertainty (estimated standard deviation) of $0.2\%/\sqrt{3}$.

### *C. Averager Linearity Deviation*

The signal averager is specified by the manufacturer to be linear to full scale within ±0.1% over the dynamic range we use. Deviations from linearity would result in a corresponding uncertainty in measured signal power. For a rectangular distribution, this corresponds to a standard uncertainty of ±0.06%.

### *D. System Internal PDL Variation*

System retardance elements contribute their own PDL (0.02 dB) to that of the DUT, but we assume it is constant during both phases of the measurement; this allows for cancellation in the ratios. However, any deviation in system PDL over the course of a measurement appears as an uncertainty in signal power. Our quoted PDL variation was derived from the maximum observed slope in measurements of the internal PDL taken over 15 min intervals. For a rectangular distribution, this corresponds to a standard uncertainty of ±0.12%.

TABLE I
ESTIMATES OF UNCERTAINTY FOR THE MUELLER–STOKES PDL MEASUREMENT SYSTEM EXPRESSED AS ONE STANDARD UNCERTAINTY ($1\sigma$). THE COMPONENTS INHERENT TO THE SYSTEM (LINES 1–4) ARE EXPRESSED AS A PERCENTAGE UNCERTAINTY IN SIGNAL POWER. THESE FOUR COMPONENTS ARE PROPAGATED AS DISCUSSED IN APPENDIX C TO YIELD THE CONTRIBUTION AS A PERCENTAGE OF MEAN PDL: THE PROPAGATED MEASUREMENT SYSTEM UNCERTAINTY. TOTAL COMBINED STANDARD UNCERTAINTIES ARE PRESENTED FOR TWO ARTIFACT CONDITIONS AND ARE CALCULATED AS ROOT-SUM-OF-SQUARES (RSS) VALUES OF THE UNCERTAINTY COMPONENTS. TWO EXAMPLES FOR THE CASE OF 0.055 dB MEAN PDL ARE CALCULATED

| Uncertainty Sources | One Standard Uncertainty |
|---|---|
| Polarization state uncertainty | ±0.83% of signal power |
| Retarder temperature dependence | ±0.12% of signal power |
| Averager linearity deviation | ±0.06% of signal power |
| System internal PDL variation | ±0.12% of signal power |
| Propagated measurement system uncertainty ($\sigma_{signal}$) | ±2.1% of PDL |
| Connector PDL uncertainty for terminated artifacts: ($\sigma_{connector} = \delta_{max}/\sqrt{3}$) | ±0.0029 dB |
| PDL measurement repeatability ($\sigma_{repeatability}$) | ±0.0008 dB |
| Combined standard uncertainty (open-beam artifact, cf. section V) | (0.0008 dB & 2.1% of PDL)RSS ($\sigma_{repeatability}$ & $\sigma_{signal}$) RSS |
| Combined standard uncertainty (pigtailed artifact, cf. Section V) | (0.0029 dB & 0.0008 dB & 2.1% of PDL)RSS ($\sigma_{connector}$ & $\sigma_{repeatability}$ & $\sigma_{signal}$) RSS |
| Example 1: Combined standard uncertainty for 0.055 dB PDL (open-beam artifact) | ±0.0014 dB |
| Example 2: Combined standard uncertainty for 0.055 dB PDL (artifact with terminated pigtailing) | ±0.0032 dB |

### *E. Propagated Measurement System Uncertainty*

We have included the four nonrandom uncertainties inherent to the measurement system (items 1–4 of the table) in a symbolic model of the nonideal system. Variations from the ideal are calculated by combining the four parameters in a root-sum-of-squares (RSS) uncertainty in signal power for each of the measured polarization states. The resulting PDL deviations are calculated from the defining equations of PDL based on (1)–(4) and the propagation relation given in Appendix C.

### *F. Connector PDL Uncertainty for Terminated Artifacts*

Connector PDL uncertainty is a combination of two components. The first is the scatter observed on PDL measurements repeated after disconnecting and reconnecting the FC/PC connectors associated with the system, DUT, and detector. The second is the net effect of multiple PDL sources in series. Any change in fiber pigtail position during a disconnection/reconnection cycle that causes a shift in fiber birefringence can dynamically alter the relative orientations of system, DUT, and termination PDL axes. Small PDL combinations with parallel axes will add approximately linearly, while those with normal axes will likewise subtract [16]. The magnitudes we report are from our own experience. A value as high as 0.05 dB is possible [10]. This effect is an issue only when testing terminated devices and is an uncertainty shared by all PDL measurement methods.

### *G. PDL Measurement Repeatability*

The repeatability given is one standard deviation ($1\sigma$) of repeated undisturbed measurements following the initial baseline measurement. By undisturbed, we mean that one sample follows another with no connector disconnection in between. This value is the effective system noise.

The effects are assumed to be uncorrelated, so we combine the results using the root-sum-of-squares method to produce a combined standard uncertainty.

## V. RESULTS

Three artifacts were chosen to test the performance of the system. The primary artifact provides a calculable PDL of moderate accuracy. It consists of an open beam launcher/collimator (a cleaved section of single-mode fiber

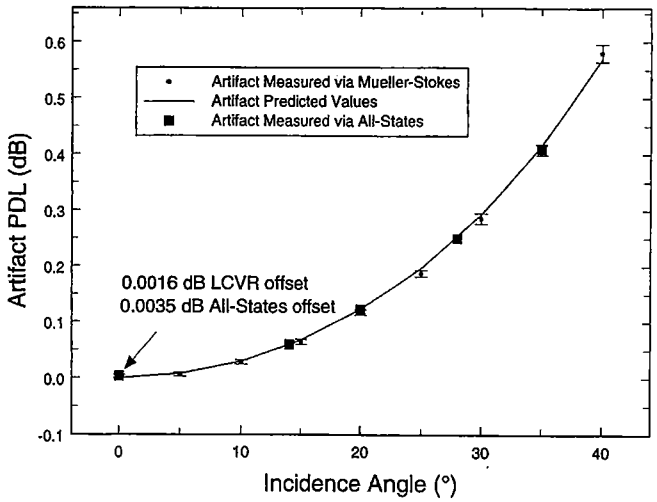


Fig. 6. Open-beam artifact data from both the Mueller–Stokes and all-states systems. Error bars represent total uncertainty. The solid line is the calculated PDL value.

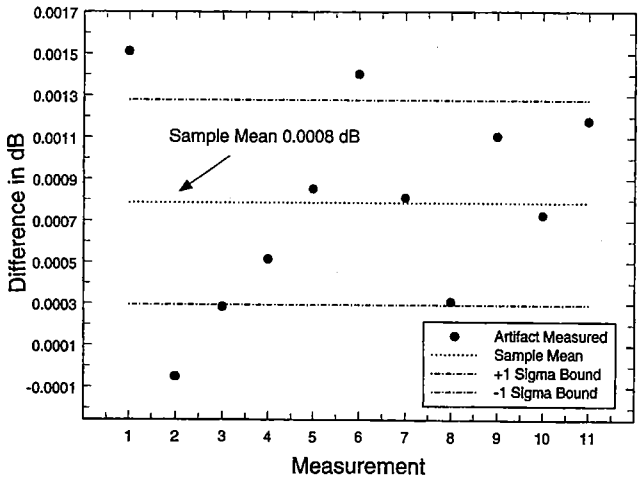


Fig. 7. Results of a resolution test using 5′ differences in optical-incidence angle on the BK7 artifact.

and objective lens) followed by a BK7 polished glass cube. We mount the cube on a rotation stage with 5′ resolution. The InGaAs detector (which includes a ceramic depolarizer) is translated to compensate for beam displacement following rotation. Our residual system PDL was measured and accounted for as a 0.0016 ± 0.0001 dB offset at normal incidence, where the uncertainty quoted is the statistical uncertainty of the mean with 95% confidence interval ($2\sigma/\sqrt{N}$). This nominally left only the dual glass/air interfaces to produce PDL. Calculated PDL (Fresnel) and measured (Mueller–Stokes) values as a function of input angle are presented in Fig. 6 and are in good agreement. Comparison measurements from an all-states technique (discussed later) are also shown.

Results of our resolution test are presented in Fig. 7. In this test, we set rotation stage to 15° for a nominally 0.0678 dB of PDL; 5 arc min of additional rotation was calculated to produce an additional 0.0008 dB of PDL. A series of Mueller–Stokes measurements was performed by alternating

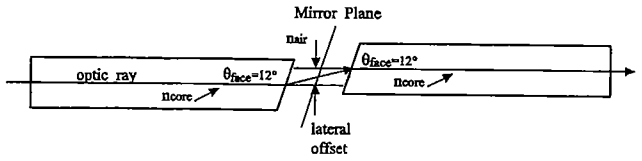


Fig. 8. Schematic representation of the controlled-air-gap connector pair artifact.

between 15° and 15°5′ and differences of each pair were taken. We found the average of those measurements, 0.0008 ± 0.0003 dB, to be in good agreement with the predicted value.

The second artifact we used is a coupled pair of commercial controlled-air-gap (CAG) fiber connectors. The CAG connector is designed for ultralow return loss and is angle-polished at 12°. The pair of CAG connectors is pigtailed with standard 9 $\mu$m single-mode fiber and terminated with FC/PC connectors. We illustrate the relevant section schematically in Fig. 8 where PDL is determined by face angle, index difference, and waveguide effects. This component was chosen to provide a readily available single-mode PDL artifact. We discovered, however, that simple plane-wave arguments do not correctly account for the measured PDL. We measure a mean PDL of 0.057 dB using the Mueller–Stokes method with reproducibility (one standard deviation) of ±0.0012 dB. A simple Fresnel coefficient calculation, however, yields 0.084 dB at this wavelength. It is possible that this discrepancy is due to waveguide effects that were not accounted for.

Our third artifact is a standard 9 $\mu$m single-mode patch cord, 15 cm in length, terminated to "ultra-polish" specifications with a FC/PC connector on one end and a standard 8° wedge FC/APC connector on the other. This device produces a mean PDL of 0.025 dB using the Mueller–Stokes method with reproducibility (one standard deviation) of ±0.0006 dB. The Fresnel PDL value calculated from the core index of refraction ($n_{\text{eff}} = 1.468$) is 0.017 dB. Again, we observe a discrepancy between the predicted and observed values, which we plan to investigate further.

For comparison, we made corroborating measurements of these three artifacts with a commercial fiber-loop polarization scanner and low-PDL optical power meter. This arrangement is depicted schematically in Fig. 9 and consists of commercially available components. The same spectrally broad ELED source is polarized using polarizing fiber and monitored by a reference detector through a 10/90 coupler. Remaining light is pseudorandomly retarded by the scanner to provide an all-polarization-states source. The output of the scanner is coupled through an FC/PC connection to the DUT. This connection serves as the test point, which will be made and broken to measure the effect of connector PDL. Detector PDL, initially less than 0.002 dB, is reduced even further by a ceramic depolarizer to less than 0.001 dB. The ceramic depolarizer is used in this case rather than the multimode device since it is better suited to the large area of the detector. Measurements consist of 500-point scans taken over 20 s with the scanner set to provide 98% coverage of the polarization space. Uncertainty in these measurements, due to imperfect sphere coverage, is estimated to be 5% [10]. We divide the detected signal by the

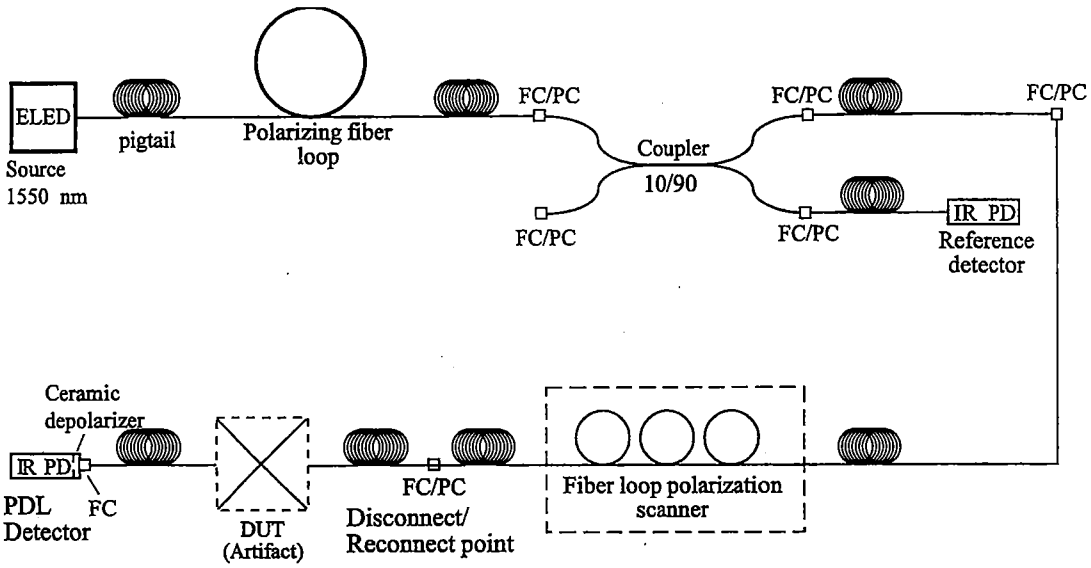


Fig. 9. Schematic representation of the all-states PDL measurement system used for intercomparison.

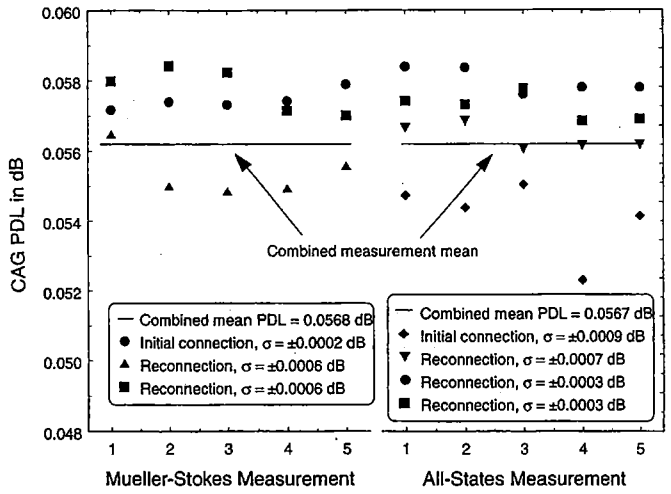


Fig. 10. Comparison of results obtained for the controlled-air-gap artifact using both the Mueller–Stokes method and the all-states technique. Standard deviations for each measurement set are given along with a combined mean. Each measurement set spans 20 s and is separated by an FC/PC connector reconnection cycle.

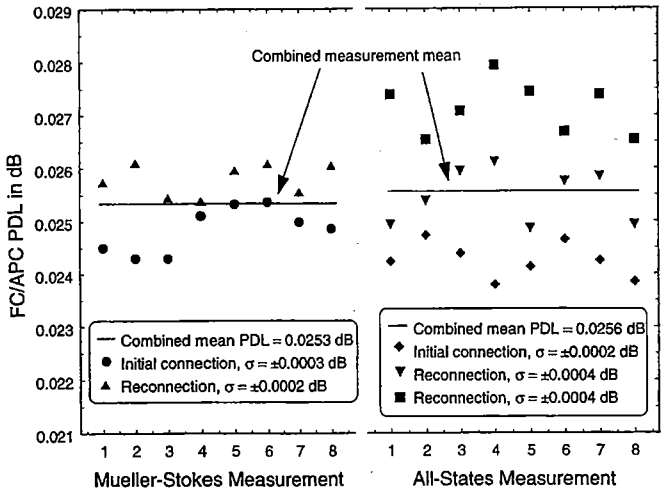


Fig. 11. Comparison of results obtained for the FC/APC patchcord artifact using both the Mueller–Stokes method and the all-states technique. Standard deviations for each measurement set are given along with a combined mean. Each measurement set is separated by an FC/PC connector reconnection cycle.

reference signal to remove the effect of power fluctuations in the polarized source.

Comparisons were made first on the controlled-air-gap device where we measured a mean PDL of 0.057 dB and reproducibility (one standard deviation) of ±0.0015 dB. Fig. 10 shows the results of the four sets using the all-states technique and three sets using the Mueller–Stokes method. The steps in the data between sets correspond to each connector reconnection cycle.

The APC artifact produced a mean PDL of 0.026 dB using the all-states technique with reproducibility (one standard deviation) of ±0.0013 dB. A comparison of the two methods on this artifact is shown in Fig. 11. Again each measurement spans 20 s and the steps in the data between sets correspond to each connection-reconnection cycle. These measurements give good agreement with the Mueller–Stokes method.

## VI. Conclusions

The nonmechanical technique of polarization dependent transmittance measurement for both single-mode and bulk-optic devices offers advantages over more traditional methods. The technique is capable of synchronous time averaging which allows resolution to better than 0.001 dB and agreement within 0.0016 dB, ±2% of PDL values calculated for an open-beam artifact. Combined mean values, calculated over several connection-reconnection cycles, agree within 1% with pseudorandom all-states measurements of a controlled-air-gap artifact and an FC/APC artifact. Additional advantages of this approach include low noise, simple calibration of spectral dependence over a broad wavelength range, and potential uses in environments otherwise unsuitable for mechanical instrumentation.

We have also conducted a detailed analysis of the possible error sources in this measurement system. For open-beam

artifacts, the accuracy is limited to the observed offset of 0.0016 dB and the 2% uncertainty inherent in the system. For low PDL measurements involving pigtailed artifacts, the accuracy is limited to ±0.003 dB, primarily due to fiber connector PDL uncertainty. For measurements of higher values of PDL, the uncertainty is dominated by the ±2% measurement system uncertainty.

The accuracy can be improved in the future by reducing the fiber connector PDL, further minimizing birefringence change during measurement, and improving the accuracy of the polarization state calibration.

## APPENDIX A
## DEPENDENCE OF PDL ON MUELLER MATRIX ELEMENTS

Information about the global transmission extrema is contained in the first-row matrix elements. The transmission $T$ is defined as the ratio of output to input Stokes vector zeroth elements

$$T \equiv \frac{S_{\text{out}_0}}{S_{\text{in}_0}} = \frac{1}{I_a}(m_{11}I_a + m_{12}I_B + m_{13}I_c + m_{14}I_d) = \frac{\mathbf{I}_{\text{in}} \cdot \mathbf{m_1}}{I_a} \tag{A1}$$

where $\mathbf{S}_{\text{in}}$ and $\mathbf{S}_{\text{out}}$ are the Stokes row vectors of input and output states identified with the corresponding power measurements $I_a \cdots I_d = S_{\text{in}_0} \cdots S_{\text{in}_3}$ and $I_1 \cdots I_4 = S_{\text{out}_0} \cdots S_{\text{out}_3}$, $\mathbf{m_1}$ is the column vector of (2) consisting of first row Mueller matrix elements and $\mathbf{I}_{\text{in}}$ is a row vector of measured input powers, $I_a \cdots I_d$. Considering the elements of $\mathbf{m_1}$ as polynomial coefficients, the transmission extrema are determined by a differential variation of each $S_{\text{in}_n}/S_{\text{in}_0}|_{n=1,2,3}$ term subject to the constraint of complete polarization

$$\left(\frac{S_{\text{in}_1}}{S_{\text{in}_0}}\right)^2 + \left(\frac{S_{\text{in}_2}}{S_{\text{in}_0}}\right)^2 + \left(\frac{S_{\text{in}_3}}{S_{\text{in}_0}}\right)^2 = 1. \tag{A2}$$

We solve this constrained optimization problem by recasting (A1) and (A2) as a Lagrange multiplier problem with the following intermediate associations:

$$\mathcal{T} \equiv m_{11} + m_{12}y_1 + m_{13}y_2 + m_{14}y_3 \tag{A3}$$

$$\psi \equiv y_1^2 + y_2^2 + y_3^2 - 1 = 0 \tag{A4}$$

where the $y_{1,2,3}$ are identified as the $S_{\text{in}_n}/S_{\text{in}_0}|_{n=1,2,3}$ terms. The Lagrange functions are then calculated from

$$L_{y_1} = \frac{\partial \mathcal{T}}{\partial y_1} + \lambda\frac{\partial \psi}{\partial y_1} = m_{12} + 2\lambda y_1 = 0$$

$$L_{y_2} = \frac{\partial \mathcal{T}}{\partial y_2} + \lambda\frac{\partial \psi}{\partial y_2} = m_{13} + 2\lambda y_2 = 0$$

$$L_{y_3} = \frac{\partial \mathcal{T}}{\partial y_3} + \lambda\frac{\partial \psi}{\partial y_3} = m_{14} + 2\lambda y_3 = 0. \tag{A5}$$

Equations (A4) and (A5) now comprise a set of four equations in four unknowns that can be solved to yield

$$y_1 = \frac{-m_{12}}{2\lambda},\ y_2 = \frac{-m_{13}}{2\lambda},\ y_3 = \frac{-m_{14}}{2\lambda} \tag{A6}$$

and therefore

$$\left[\frac{m_{12}}{2\lambda}\right]^2 + \left[\frac{m_{13}}{2\lambda}\right]^2 + \left[\frac{m_{14}}{2\lambda}\right]^2 = 1. \tag{A7}$$

Solving for $\lambda$ and substituting it back into $\mathcal{T}$ (and hence $T$) yields the transmitted power extrema as

$$T_{\max} = m_{11} + \sqrt{m_{12} + m_{13} + m_{14}}$$

$$T_{\min} = m_{11} - \sqrt{m_{12} + m_{13} + m_{14}} \tag{A8}$$

corresponding to the two roots of $\lambda$. Polarization dependent loss (in dB) is defined as the ratio

$$\text{PDL} \equiv 10\log\left[\frac{T_{\max}}{T_{\min}}\right]. \tag{A9}$$

For additional detail, refer to Favin *et al.* [13].

## APPENDIX B
## INPUT STOKES VECTOR $\mathbf{S}_{\text{in}}$ DEPENDENCE ON LCVR RETARDANCE

We begin by noting the matrix forms of each component in the optical train: a linear polarizer, LCVR modulator 1, and LCVR modulator 2. The Mueller matrix for an ideal linear polarizer with transmission axis set at angle $\theta$ is given as

$$\mathbf{M}_p(\theta) = \frac{1}{2}\begin{bmatrix} 1 & \cos(2\theta) & \sin(2\theta) & 0 \\ \cos(2\theta) & \cos^2(2\theta) & \sin(2\theta)\cos(2\theta) & 0 \\ \sin(2\theta) & \sin(2\theta)\cos(2\theta) & \sin^2(2\theta) & 0 \\ 0 & 0 & 0 & 0 \end{bmatrix} \tag{B1}$$

while the corresponding matrix for an ideal retarder of phase shift $\phi$ and fast axis angle $\theta$ is shown in (B2) at the bottom of the page. Now, consider an arbitrary input polarization state normalized to produce unit output when linearly polarized

$$\mathbf{S}_0 = \frac{2}{\left[1 + \frac{1}{\sqrt{3}}\right]} \cdot \begin{bmatrix} 1 \\ 1/\sqrt{3} \\ 1/\sqrt{3} \\ 1/\sqrt{3} \end{bmatrix} \tag{B3}$$

such that when multiplied by the system matrix $\mathbf{M}_s = \mathbf{M}_r(\phi_2, 0)\mathbf{M}_r(\phi_1, \pi/4)\mathbf{M}_p(0)$ for the present arrangement, that is

$$\mathbf{M}_s(\phi_1, \phi_2) = \frac{1}{2}\begin{bmatrix} 1 & 1 & 0 & 0 \\ \cos(\phi_1) & \cos(\phi_1) & 0 & 0 \\ \sin(\phi_1)\sin(\phi_2) & \sin(\phi_1)\sin(\phi_2) & 0 & 0 \\ -\sin(\phi_1)\cos(\phi_2) & -\sin(\phi_1)\cos(\phi_2) & 0 & 0 \end{bmatrix} \tag{B4}$$

$$\mathbf{M}_r(\phi, \theta) = \begin{bmatrix} 1 & 0 & 0 & 0 \\ 0 & \cos^2(2\theta) + \cos(\phi)\sin^2(2\theta) & (1 - \cos(\phi))\sin(2\theta)\cos(2\theta) & \sin(\phi)\sin(2\theta) \\ 0 & (1 - \cos(\phi))\sin(2\theta)\cos(2\theta) & \sin^2(2\theta) + \cos(\phi)\cos^2(2\theta) & -\sin(\phi)\cos(2\theta) \\ 0 & -\sin(\phi)\sin(2\theta) & \sin(\phi)\cos(2\theta) & \cos(\phi) \end{bmatrix}. \tag{B2}$$

produces a new Stokes vector with the following dependence on the phase shifts of the two retarders:

$$S_{\text{in}}(\phi_1, \phi_2) = \begin{bmatrix} 1 \\ \cos(\phi_1) \\ \sin(\phi_1)\sin(\phi_2) \\ -\sin(\phi_1)\cos(\phi_2) \end{bmatrix} \tag{B5}$$

which is the field incident on the DUT.

## APPENDIX C
## PROPAGATION OF UNCERTAINTY

Variations in power due to effects outlined in the first four rows of Table I contribute uncorrelated uncertainties to the Stokes power information contained in $I_a \cdots I_d$ and $I_1 \cdots I_4$ and propagated according to

$$\sigma_{\text{signal}} = \sqrt{\sum_{a,b,c,d} \left(\frac{\partial \text{PDL}}{\partial I_i}\right)^2 \delta_{I_i}^2 + \sum_{1,2,3,4} \left(\frac{\partial \text{PDL}}{\partial I_i}\right)^2 \delta_{I_i}^2} \tag{C1}$$

where $\sigma_{\text{signal}}$ refers to one standard deviation in PDL and $\delta_I$ refers to standard uncertainties in state powers for the case of independent measurements. The partial derivatives, in our case, are calculated symbolically according to (1)–(4) of Section II.

## ACKNOWLEDGMENT

The authors express their sincere appreciation to J. Wang of NIST/ITL for assistance and L. Stokes of the HP Lightwave Division for helpful discussions. In addition, they thank the HP Lightwave Division for the loan of equipment for our comparative measurements.

## REFERENCES

[1] E. Lichtmann, "Performance degradation due to polarization dependent gain and loss in lightwave systems with optical amplifiers," *Electron. Lett.*, vol. 29, pp. 1969–1970, Oct. 1993.
[2] F. Bruyére and O. Audouin, "Penalties in long-haul optical amplifier systems due to polarization dependent loss and gain," *IEEE Photon. Technol. Lett.*, vol. 6, pp. 654–656, May 1994.
[3] K. Kikushima, K. Suto, H. Yoshinaga, and E. Yoneda, "Polarization dependent distortion in AM-SCM video transmission systems," *J. Lightwave Technol.*, vol. 12, pp. 650–657, Apr. 1994.
[4] H. Poincaré, *Théorie Mathématique de la Lumiére.* Paris, France: Georges Carré, 1892, pp. 275–285.
[5] E. Collett, *Polarized Light Fundamentals and Applications.* New York: Marcell-Decker, 1993, pp. 219–253.
[6] E. Lichtmann, "Limitations imposed by polarization-dependent gain and loss on all-optical ultralong communication systems," *J. Lightwave Technol.*, vol. 13, pp. 906–913, May 1995.
[7] A. Mabrouki, M. Gadonna, and R. Le Naour, "Analysis and measurement of the polarization sensitivity of single-mode fiber passive optical components," *Fiber Integrated Opt.*, vol. 15, pp. 15–26, 1996.
[8] M. Gadonna and A. Mabrouki, "Polarization sensitivity measurements methods for passive optical components," in *Conf. European Fiber Optic Commun. Networks, EFOC&N'93, Tech. Dig.*, The Hague, The Netherlands, pp. 65–67.
[9] N. Mekada, A. Al-Hamdan, T. Murakami, and M. Miyoshi, "New direct measurement technique of polarization dependent loss with high resolution and repeatability," in *Tech. Dig., Symp. Optic. Fiber Measurements, SOFM'94,* Boulder, CO, pp. 189–192.
[10] Hewlett-Packard, *Polarization-Dependent Loss Measurements,* Hewlett-Packard Product Note 11896-1.
[11] B. Nyman and G. Wolter, "High-resolution measurement of polarization dependent loss," *IEEE Photon. Technol. Lett.*, vol. 5, pp. 817–818, July 1993.
[12] B. L. Heffner, "Deterministic, analytically complete measurement of polarization-dependent transmission through optical devices," *IEEE Photon. Technol. Lett.*, vol. 4, pp. 451–454, May 1992.
[13] D. L. Favin, B. M. Nyman, and G. Wolter, "System and method for measuring polarization dependent loss," U.S. Patent 5 371 597, Dec. 6, 1994.
[14] B. M. Nyman, D. L. Favin, and G. Wolter, "Automated system for measuring polarization dependent loss," in *Tech. Dig., Optic. Fiber Commun. Conf., OFC'94,* San Jose, CA, pp. 230–231.
[15] S. Wu, *Electro-Optics of Nematic Liquid Crystals, Handbook of Optics.* New York: McGraw-Hill, 1996, vol. 2, ch. 14.5.
[16] N. Gisin, "The statistics of polarization dependent losses," in *Tech. Dig., Symp. Optic. Fiber Measurements, SOFM'94,* Boulder, CO, pp. 193–196.
[17] M. W. Maeda and D. A. Smith, "New polarization-insensitive detection scheme based on fiber polarization scrambling," *Electron. Lett.*, vol. 27, no. 1, pp. 10–12, Jan. 1991.
[18] B. N. Taylor and C. E. Kuyatt, "Guidelines for evaluating and expressing the uncertainty of NIST measurement results," *Nat. Inst. Stand. Technol.*, Tech. Note 1297, 1994.

**Rex M. Craig** received B.S. degrees in physics and mathematics in 1982 and the M.S. degree in physics from the University of Colorado, Boulder, in 1986.

Since 1987, he has worked with the Electromagnetic Technology Division and has been with the Optoelectronics Division of the National Institute of Standards and Technology (NIST), Boulder, CO. He has conducted research in cryogenic optical radiometry, cryogenic optical calorimetry, fiber component polarimetry, optical depolarization, and sensor fiber properties. In 1993, he joined the Optical Components Group and conducts research in polarization dependence metrology and sensor fiber metrology. He is active in national fiber-optic telecommunication standards efforts and participates in or chairs several associated committees.

**Sarah L. Gilbert** received the B.S. degree in physics from the University of Hawaii, Honolulu, in 1978 and the Ph.D. degree in physics from the University of Michigan, Ann Arbor, in 1984.

After graduating, she was an NRC Postdoctoral Research Fellow with the Ion Storage Group in the National Bureau of Standards Time and Frequency Division. She is currently Group Leader of the Optical Components Group in the National Institute of Standards and Technology (NIST) Optoelectronics Division. Her research areas are wavelength standards for optical fiber communications and metrology for optical fiber components, such as Bragg fiber gratings.

Dr. Gilbert was awarded the Department of Commerce Bronze medal for her wavelength standards work. She is a member of the American Physical Society and the Optical Society of America (OSA).

**Paul D. Hale** received the B.S. degree in engineering physics in 1985 and Ph.D. degree in applied physics from the Colorado School of Mines, Golden, in 1989.

Since 1989, he has worked with the Optoelectronics Division of the National Institute of Standards and Technology (NIST), Boulder, CO. He has conducted research in birefringent devices, mode-locked fiber lasers, fiber chromatic dispersion, broad-band lasers, interferometry, polarization standards, optical noise, photodiode frequency response, and high-speed measurements. He is presently leader of the High Speed Measurements Project in the Sources and Detectors Group. He has authored or coauthored over 23 publications and two NIST Standard Reference Materials

Dr. Hale received the U.S. Department of Commerce Gold Medal, along with a team of four other scientists, for measuring fiber cladding diameter with an uncertainty of 30 nm in 1994. He is a member of the Optical Society of America (OSA).